

REDUCED PEEC MODELING OF WIRE-GROUND STRUCTURES USING A SELECTIVE MESH APPROACH

Z. F. Song^{1,*}, F. Dai¹, D. L. Su¹, S. G. Xie¹, and F. Duval²

¹School of Electronics and Information Engineering, Beihang University, Beijing 100191, China

²IRSEEM, ESIGELEC, Saint Etienne du Rouvray 76801, France

Abstract—The wire-ground electromagnetic coupling structures are quite common in avionics system electromagnetic compatibility (EMC) analysis. The increasing complexities of physical structures make electromagnetic modeling an increasingly tough task, and computational efficiency is desirable. In this paper, a novel selective mesh approach is presented for partial element equivalent circuit (PEEC) modeling where intense coupling parts are meshed while the remaining parts are eliminated. With the proposed approach, the meshed ground plane is dependent on the length and height of the above wires. Relevant compact formulae for determining mesh boundaries are deduced, and a procedure of general mesh generation is also given. A numerical example is presented, and a validation check is accomplished, showing that the approach leads to a significant reduction in unknowns and thus computation time and consumed memories, while preserving the sufficient precision. This approach is especially useful for modeling the electromagnetic coupling of wires and reference ground, and it may also be beneficial for other equivalent circuit modeling techniques.

1. INTRODUCTION

With the development of avionics and system integration techniques, electromagnetic environment in aircraft cabins becomes more and more severe and complicated due to rich spectrum and limited space. Electromagnetic compatibility (EMC) is now becoming one of the key abilities guaranteeing avionics systems' normal

Received 21 November 2011, Accepted 23 December 2011, Scheduled 31 December 2011

* Corresponding author: Zhenfei Song (songzhenfei@gmail.com).

performances without suffering unacceptable degradation or causing unintentional degradation [1–4]. Wire connection is an important medium for necessary signal and power transmission. However, unreasonable wiring or incorrect wire connection provides an undesired electromagnetic interference (EMI) coupling path to the subsystems or equipments. It is reported that most of the performance degradation of equipments or systems results from electromagnetic coupling via wires/cables [5–8].

Reasonable wiring is an important content to heighten EMC of a complex avionics system [9]. This paper is dedicated to effective modeling of wire-ground structures. By the term “wire-ground structure”, we mean a typical electromagnetic coupling structure of a ground plane associated with a wire/cable suspended over it. This structure is quite common in avionics system EMC analysis.

Currently, the partial element equivalent circuit (PEEC) method [10], firstly introduced by Ruehli in 1970s, is one of the promising numerical methods for electromagnetic (EM) modeling of various engineering problems, e.g., EMC, EMI and signal and power integrity (SI, PI) of high-speed digital circuits [11–13]. This method facilitates a combination of circuit and electromagnetic analysis because a circuit interpretation of the electric field integral equation (EFIE) in terms of partial circuit elements, namely resistances, partial inductances, and partial coefficients of potentials can be achieved [14]. Different from other integral equation (IE) based EM modeling methodologies, PEEC is a full spectrum method valid from dc to maximum frequency determined by mesh. The PEEC method is implemented for modeling wire-ground structures thanks to its potentials for mixed electromagnetic-circuit problems.

The term “mesh” is a discretization of a geometric domain into small elementary cells, such as triangles or quadrilaterals in two dimensions and tetrahedral or hexahedral elements in three [15]. The meshing of geometrical objects is a first step in EM modeling using numerical techniques, and the overall solution efficiency strongly depends on the geometrical mesh algorithms [15–17]. The majority of the PEEC implementations mesh surfaces using quadrilateral elements and volume cells are created as hexahedral cells. The basic rule of thumb when carrying out discretization for PEEC modeling is to use a fixed number of cells per shortest wavelength λ_{\min} corresponding to the highest frequency of interest [18]. Following this conventional solution, excessive number of unknowns and subdivisions will be introduced, especially for large structures at high frequencies.

Several procedures aimed at minimizing the complexity of the meshing while preserving sufficient accuracy have been devel-

oped [14, 17, 19]. Some non-uniform mesh procedures are developed for capturing skin effect, calculating capacitance and inductance. A α -projection algorithm for neighboring conductors is presented in [17]. However, it is not clear in setting α value. In addition, the increasing size of mesh suffers from difficulties of the node connection, and remedying strategies of smoothing, tolerating and node relaxation unavoidably influence the overall accuracy. Clearly, most of the current mesh procedures are short of considerations of coupling among elements. They all have a large number of unknowns for large structures at high frequencies, which makes time-tedious and computationally expensive modeling. The proposed mesh algorithm starts with descriptions of field distribution induced by a filament over a ground conductor. Based on the distribution characteristics, a selective mesh procedure is developed to reduce the number of unknowns.

This paper is organized as follows. An overview of PEEC modeling is presented in Section 2, including the basic PEEC formulations and meshing issues. Mathematic preliminary and the proposed selective mesh approach together with the working flow for the code implementation are described in detail in Section 3. Section 4 gives a numerical experiment where a serpentine wire suspended over a ground conductor is modeled using the proposed mesh approach. Comparison with conventional solutions and the relevant measurement results are presented in this section. Finally, Section 5 ends with conclusions.

2. OVERVIEW OF PEEC MODELING

2.1. Partial Element Equivalent Circuit Construction

The formulation of PEEC method starts with a mixed potential equation which is written as

$$\mathbf{E}^i(\mathbf{r}, t) = \frac{\mathbf{J}(\mathbf{r}, t)}{\sigma} + \frac{\partial \mathbf{A}(\mathbf{r}, t)}{\partial t} + \nabla \Phi(\mathbf{r}, t); \quad (1)$$

where \mathbf{E}^i is an incident electric field and \mathbf{J} the current density in the conductor. The potentials \mathbf{A} and Φ are, respectively, the magnetic vector potential and electric scalar potential, and σ is the electrical conductivity.

The closed forms of magnetic vector potential $\mathbf{A}(\mathbf{r}, t)$ due to current $\mathbf{J}(\mathbf{r}, t)$ and electric scalar potential $\Phi(\mathbf{r}, t)$ due to charge distribution $\rho(\mathbf{r}, t)$ are defined as

$$\mathbf{A}(\mathbf{r}, t) = \frac{\mu}{4\pi} \int_{V'} \frac{\mathbf{J}(\mathbf{r}', t')}{|\mathbf{r} - \mathbf{r}'|} dV'; \quad (2)$$

$$\Phi(\mathbf{r}, t) = \frac{1}{4\pi\epsilon} \int_{S'} \frac{\rho(\mathbf{r}', t')}{|\mathbf{r} - \mathbf{r}'|} dS'. \quad (3)$$

In (2) and (3), μ is permeability, and ϵ is permittivity, or electric constant. The t' denotes the time when the current and charge distribution. \mathbf{J} and ρ act as sources of \mathbf{A} and Φ respectively. The difference between t' and t is due to a finite value of the speed of light in the background homogenous medium. This fact results in a retarded time given by

$$\tau = t' - t = |\mathbf{r} - \mathbf{r}'|/c; \quad (4)$$

where $c = 1/\sqrt{\mu\epsilon}$.

If we substitute the potential expressions (2) and (3) into potential Equation (1), the electric field integral equation can be obtained as

$$\mathbf{E}^i(\mathbf{r}, t) = \frac{\mathbf{J}(\mathbf{r}, t)}{\sigma} + \frac{\partial}{\partial t} \frac{\mu}{4\pi} \int_{V'} \frac{\mathbf{J}(\mathbf{r}', t')}{|\mathbf{r} - \mathbf{r}'|} dV' + \frac{1}{4\pi\epsilon} \nabla \int_{S'} \frac{\rho(\mathbf{r}', t')}{|\mathbf{r} - \mathbf{r}'|} dS'. \quad (5)$$

To ensure the conservation of charge, the continuity equation should be enforced:

$$\nabla \cdot \mathbf{J}(\mathbf{r}, t) + \frac{\partial \rho(\mathbf{r}, t)}{\partial t} = 0. \quad (6)$$

Equations (5) and (6) can be rewritten in the Laplace domain as:

$$\begin{aligned} \mathbf{E}^i(\mathbf{r}, s) &= \frac{\mathbf{J}(\mathbf{r}, s)}{\sigma} + \frac{\mu s}{4\pi} \int_{V'} \frac{\mathbf{J}(\mathbf{r}', s)e^{-s\tau}}{|\mathbf{r} - \mathbf{r}'|} dV' \\ &+ \frac{1}{4\pi\epsilon} \nabla \int_{S'} \frac{\rho(\mathbf{r}', s)e^{-s\tau}}{|\mathbf{r} - \mathbf{r}'|} dS'; \end{aligned} \quad (7)$$

$$\nabla \cdot \mathbf{J}(\mathbf{r}, s) + s\rho(\mathbf{r}, s) = 0. \quad (8)$$

PEEC method can be implemented for transient analysis by solving (5) and (6), and the solutions can also be found in the frequency domain as (7) and (8), assuming $s = j\omega$. The unknowns of such a problem are represented by the current density $\mathbf{J}(\mathbf{r}, t)$ in the interior of conductors, and the charge density $\rho(\mathbf{r}, t)$ on the surface of conductors.

The most popular method for discretization of integral equations is the method of moment (MoM) [20]. The EFIE (7) and continuity Equation (8) are spatially discretised applying the Galerkin method [21]. The basis function $\mathbf{b}_n(\mathbf{r})$ and $p_m(\mathbf{r})$ are introduced for the unknown quantities \mathbf{J} and ρ [12, 22].

$$\mathbf{J}(\mathbf{r}, \omega) = \sum_{n=1}^{N_v} \mathbf{b}_n(\mathbf{r}) I_n(\omega); \quad (9)$$

$$\rho(\mathbf{r}, \omega) = \sum_{m=1}^{N_s} p_m(\mathbf{r}) Q_m(\omega); \quad (10)$$

Here N_v and N_s represent the number of corresponding basis functions, i.e., the meshed volume and surface cells.

Piecewise constant set of basis functions as (11) and (12) are usually applied in PEEC method [12], where a_n is the cross section of volume V_n , \hat{i}_n the unit vector indicating the current orientation in volume V_n , and s_m the area of surface cell S_m .

$$\mathbf{b}_n(\mathbf{r}) = \begin{cases} \frac{\hat{i}_n}{a_n} & \mathbf{r} \in V_n \\ 0 & \text{otherwise} \end{cases} ; \quad (11)$$

$$p_m(\mathbf{r}) = \begin{cases} \frac{1}{s_m} & \mathbf{r} \in S_m \\ 0 & \text{otherwise} \end{cases} . \quad (12)$$

Such a basis function selection results in physical meaning of the corresponding basis function weights. $I_n(\omega)$ represents the current flowing in the volume V_n , and $Q_m(\omega)$ is the charge on the surface element S_m .

With definitions of partial inductance in (13) and resistance in (14), EFIE can be interpreted as a circuit Equation (15) by enforcing Kirchhoff's voltage law (KVL) in resistive-inductive (R - L) branches between coupled nodes.

$$Lp_{in} = \frac{\mu}{4\pi} \frac{1}{a_i a_n} \int_{V_i} \int_{V_n} \hat{i}_i \cdot \hat{i}_n \frac{e^{-j\omega\tau}}{|\mathbf{r}_i - \mathbf{r}_n|} dV_n dV_i; \quad (13)$$

$$R_i = \frac{l_i}{\sigma a_i}; \quad (14)$$

$$\Phi_{1i}(\omega) - \Phi_{2i}(\omega) = V_i^i(\omega) + R_i I_i + j\omega \sum_{n=1}^{N_v} Lp_{in} I_n(\omega); \quad (15)$$

where $V_i^i(\omega)$ represents a voltage source due to external field; Φ_{1i} and Φ_{2i} are potentials at two terminals of volume V_i . In a PEEC circuit network, (15) can be rewritten in a compact matrix form as

$$\mathbf{A}\Phi(\omega) + \mathbf{R}\mathbf{I}(\omega) + j\omega\mathbf{L}\mathbf{P}(\omega)\mathbf{I}(\omega) + \mathbf{V}^i(\omega)=0. \quad (16)$$

The entries in the connectivity matrix \mathbf{A} are defined as

$$a_{nk} = \begin{cases} +1 & \text{if current flows from node } k \text{ to } n \\ -1 & \text{if current flows from node } n \text{ to } k \\ 0 & \text{others} \end{cases} .$$

With the definition of partial coefficient of potential in (17), the electric scalar potential $\Phi(\omega)$ defined by (3) is related to the charges located on the meshed surface patches as (18).

$$P_{lm}(\omega) = \frac{1}{4\pi\epsilon} \frac{1}{s_m} \frac{1}{s_l} \int_{s_m} \int_{s_l} \frac{e^{-j\omega\tau}}{|\mathbf{r}_l - \mathbf{r}_m|} ds_m ds_l; \quad (17)$$

$$\Phi(\omega) = \mathbf{P}(\omega)\mathbf{Q}(\omega). \quad (18)$$

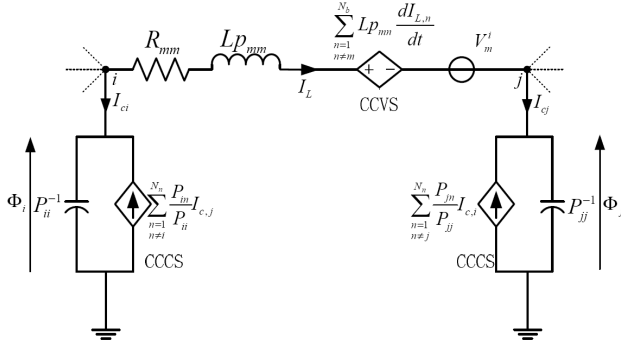


Figure 1. Elementary partial element equivalent circuit model.

The PEEC method enforces the continuity Equation (6) at equivalent circuit nodes in form of Kirchhoff’s current law (KCL) as

$$\mathbf{I}_c(\omega) - \mathbf{A}^T \mathbf{I}_L(\omega) = \mathbf{I}_s(\omega); \tag{19}$$

where $\mathbf{I}_c(\omega) = j\omega\mathbf{Q}(\omega)$ is the displacement current in capacitive branches; $\mathbf{I}_L(\omega)$ is the current in R - L branches; $\mathbf{I}_s(\omega)$ represents the external current sources connecting to the nodes.

Circuit Equations (16) and (18) represent magnetic and electric field couplings, respectively, thus leading to an elementary equivalent circuit as in Fig. 1, which is called partial element equivalent circuit.

The resulting equivalent circuit illustrated in Fig. 1 is suitable for being solved by appropriate network solver. The modified nodal analysis (MNA) [23] circuit Equation (20) can be applied in frequency domain.

$$\begin{bmatrix} -(\mathbf{R} + j\omega\mathbf{L}_p) & -\mathbf{A} \\ -\mathbf{A}^T & j\omega\mathbf{P}^{-1} \end{bmatrix} \begin{bmatrix} \mathbf{I}_L \\ \Phi \end{bmatrix} = \begin{bmatrix} \mathbf{V}^i \\ \mathbf{I}_s \end{bmatrix}. \tag{20}$$

2.2. Meshing for the PEEC Model

Meshing is an important issue in accurate and effective PEEC modeling, as other numerical methods [24]. Two kinds of discretizations are constructed in this method. After the initial node placement, surfaces are meshed using quadrilateral elements from which coefficients of potentials are calculated using (17). Depending on the boundaries of the surface mesh, volume cells are created as hexahedral cells from which partial inductances and resistances are calculated using (13) and (14), respectively [18]. It facilitates the partial elements calculation using such quadrilateral and hexahedral elements in the mesh [25, 26].

Figure 2(a) shows the elementary surface and volume discretization in three dimensions, where the numbers 0 ~ 6 denote the different surfaces, and I ~ VI are the volume cells. Fig. 2(b) presents the node placement of a three dimensional conductor. Three kinds of nodes are set including one inner node as (1), six surface nodes as (2), eight vertex nodes as (3), and 12 edge nodes as (4). Totally, 27 nodes are obtained. With such node placement, 54 surface cells ($6 \times 1 + 8 \times 3 + 12 \times 2 = 54$) are formed as in Fig. 2(c) indicated with different patterns. Fig. 2(d) shows two volume cells, and actually 18 such volumes cells are created in one current orientation by any two adjacent nodes. This results in 54 volumes in total in an ordinary 3-D orthogonal coordinate system [27].

The basic rule of thumb when carrying out the PEEC discretization is to use a fixed number of cells per shortest wavelength λ_{\min} (corresponding to the highest frequency of interest) to assure sufficient accuracy. Originally, approximately 10 cells per λ_{\min} was

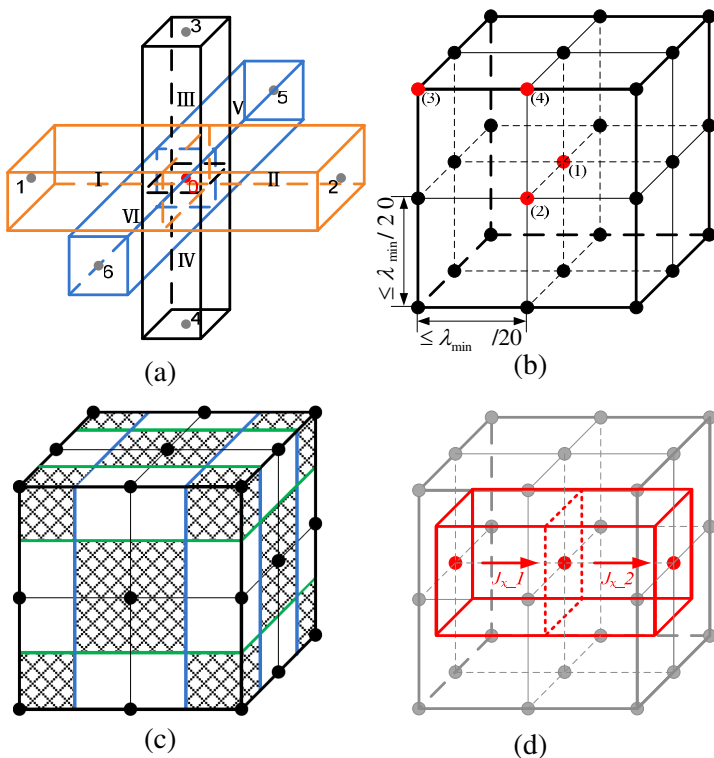


Figure 2. Surface- and volume- mesh of a rectangular structure (a) elementary mesh; (b) node placement; (c) surface cells; (d) volume cells.

used. This has been refined to 20 cells/ λ_{\min} for an improved performance in current PEEC models [15].

3. A NOVEL SELECTIVE MESH APPROACH

3.1. Wire-ground Coupling

It is well known from Biot-Savart law [28] that the magnetic field \mathbf{B} at any point P induced by an infinite filament with a time-varying current $I(t)$ can be calculated by

$$\mathbf{B} = \frac{\mu_0 I(t)}{2\pi r_0} \times \hat{r}; \quad (21)$$

where r_0 is the distance between investigated point P and the filament. \hat{r} is the displacement unit vector pointing from the wire element towards the point at which the field is being computed.

In a general orthogonal x, y, z coordinate system shown in Fig. 3, an infinite filament extending along the y coordinate is allocated with a height of h in z direction. Using (21), the induced magnetic field \mathbf{B} over the XY plane can be deduced.

$$\mathbf{B} = \hat{i}_x \frac{\mu_0 h I(t)}{2\pi(h^2 + x^2)} + \hat{i}_z \frac{\mu_0 x I(t)}{2\pi(h^2 + x^2)}. \quad (22)$$

The magnetic field has two orthogonal components as indicated in (22). Suppose that an infinite grounded conductor is allocated on the XY plane, it can be deduced with image theory that the total induced magnetic field only has the X components, and (23) is a representation of total field in presence of the conductor.

$$\mathbf{B} = \hat{i}_x \frac{\mu_0 I(t) h}{\pi(h^2 + x^2)}. \quad (23)$$

It is clear in (23) that the magnetic field is independent from the y coordinate value (height), and maximizes at $x = 0$. The field strength has quadratic falloff with the absolute value of x . Fig. 3 also illustrates the field distribution over the ground surface. Following this derivation, a similar electric field distribution can be obtained. All the derivation above is based on the assumption of infinite dimensions. However, the field distribution characteristic is acceptable for approximation in practice of large system problems. Fig. 4 shows the calculated field distribution over cross section of a wire-ground structure by MoM.

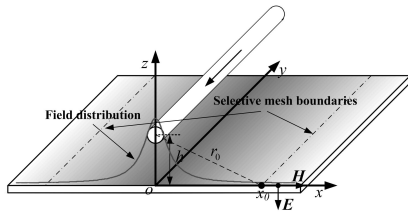


Figure 3. Description of the selective mesh.

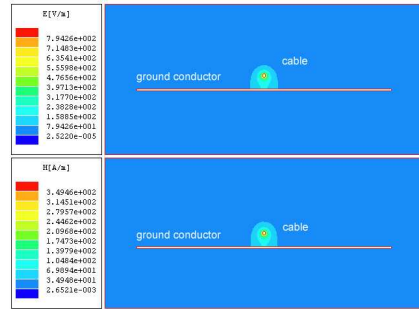


Figure 4. Field distribution over cross sections calculated by MoM.

3.2. A Selective Mesh Approach

The magnetic field \mathbf{H} indicates the inductive coupling, while the electric field \mathbf{E} represents the capacitive coupling. Since most of coupling energy is concentrated in a limited region, only intense coupling parts are meshed in the proposed selective mesh approach, while the other parts are eliminated. This can reduce the computational time and consumed memory.

Here we set mesh boundaries in both sides of a filament, and conventional mesh will be carried out only within the boundaries. The following problem is to quantitatively determine the mesh boundaries.

$$\int_0^{x_0} B(x)dx = k \int_0^{\infty} B(x)dx. \quad (24)$$

A threshold value k which means the occupation of field within the boundaries over the total field in free space is defined in (24). The threshold value is user-defined which determines the approximation accuracy, and normally a larger value of k results in a better approximation. Numerical validations indicate that a value larger than 0.9 is suitable for most practical problems. It is not difficult to solve the value of x_0 in (24), and it is a compact function of the height h and the threshold value k , as shown in (25).

$$x_0 = \tan\left(k \cdot \frac{\pi}{2}\right) \cdot h \quad (0 < k < 1). \quad (25)$$

It is evident in (25) that, with the selective mesh approach, the necessary mesh boundaries of ground plane are dependent on height and the length of the above wires. In some wire-ground structures where the ground conductor is relatively much larger than the mesh

region defined by (25), meshing the entire structure in a conventional manner with an identical discretization size is not effective.

Figure 5 illustrates a framework of the proposed mesh generation, and the process is detailed taking a wire-ground configuration in Fig. 6 as an example.

1) Count the number of straight wire segments (S_w) and flat planes (S_p). The notation $w_x^{(i)}$, $w_y^{(j)}$, and $w_z^{(k)}$ are used to identify wire segments, and $P_{XY}^{(l)}$, $P_{XZ}^{(m)}$, $P_{YZ}^{(n)}$ to name different planes. The counters i, j, k, l, m, n all start with one. So, $S_w = i + j + k$ and $S_p = l + m + n$. In a configuration of Fig. 6, $S_w = S_p = 3$.

2) Calculate the distances of wire-plane pair indicated in Table 1.

3) Calculate the mesh boundaries of each non-perpendicular wire-plane pair using (25).

4) Overlapping process. Once the selective mesh surfaces are overlapped, the overlapping subdivisions are merged as presented in Fig. 6.

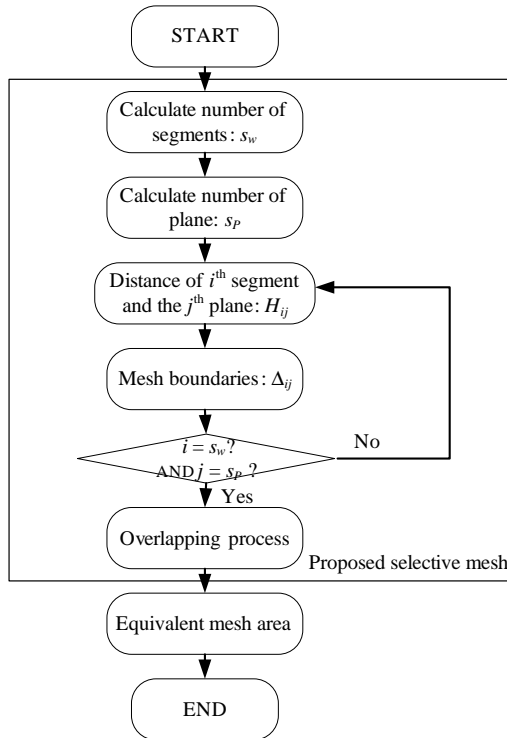


Figure 5. Framework of the proposed mesh generation.

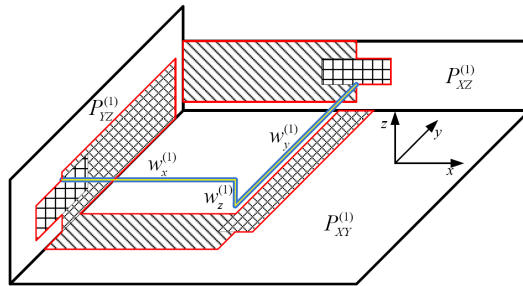


Figure 6. Equivalent mesh area by overlapping process.

Table 1. Parameters for the selective mesh.

wire \ plane	$P_{XY}^{(l)}$	$P_{XZ}^{(m)}$	$P_{YZ}^{(n)}$
$w_x^{(i)}$	$H_{x-XY}^{(i,l)}$	$H_{x-XZ}^{(i,m)}$	—
$w_y^{(j)}$	$H_{y-XY}^{(j,l)}$	—	$H_{y-YZ}^{(j,n)}$
$w_z^{(k)}$	—	$H_{z-XZ}^{(k,m)}$	$H_{z-YZ}^{(k,n)}$

4. NUMERICAL RESULTS

A serpentine wire with identical cross sectional dimensions of 1 mm × 1 mm is suspended over a ground conductor with a height of 5 mm. The ground conductor is a flat copper with the dimensions of 1 m in length, 0.5 m in width, and 0.5 mm in thickness. The wire is terminated with a 50 Ω loading in one end and excited by an ideal current source in the other. Fig. 7 and Fig. 8 are respectively the relevant dimension description and the prototype of measurement platform.

Figure 9(a) shows the conventional (full) mesh results, while Fig. 9(b) illustrates the reduced mesh results using Matlab. Here a suitable threshold value k in (25) ($k = 0.95$) is adopted to calculate the mesh boundaries.

The input impedance is a key parameter for capturing the transmission characteristics [29, 30]. In the numerical validation, the input impedance calculation is carried out to show the effectiveness of the proposed mesh procedure. The investigated frequencies are limited up to 600 MHz by a mesh size of 0.05 m.

Figure 10 presents numerical results of equivalent circuit models constructed by the full mesh and the reduced mesh approach, respectively. Excellent agreements are achieved with a suitable threshold value $k = 0.95$.

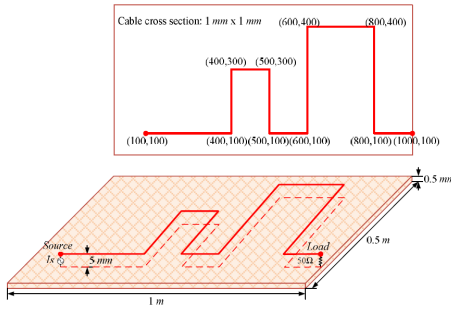


Figure 7. A serpentine wire over a ground conductor (a) 3D view; (b) dimensions.

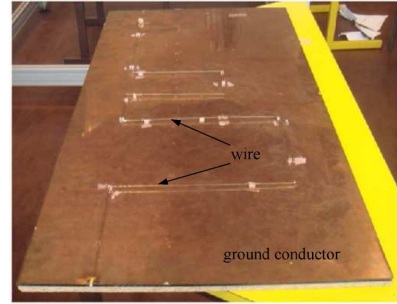


Figure 8. Prototype of measurement platform of a serpentine wire.

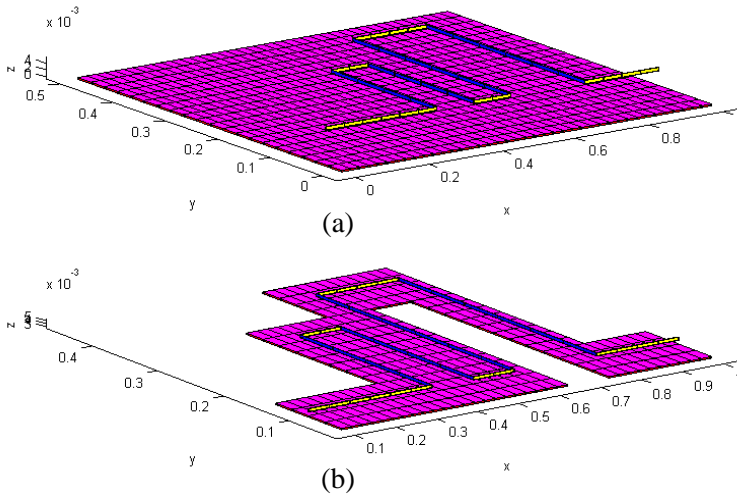


Figure 9. Meshed structures by (a) full mesh, and (b) selective mesh.

Relevant measurement results by a vector network analyzer (VNA) are also given as a reference in Fig. 10. With the increase of analysis frequencies, the meshed element dimensions reach several or even hundreds times of the shortest wavelength, so a rigorous, full-wave PEEC model is necessary, where the retarded factor τ due to wave propagation in (4) is considered [31]. Since our PEEC modeling code at present is mainly based on the quasi-static PEEC model, some difference between measurements and calculations presents at high frequencies.

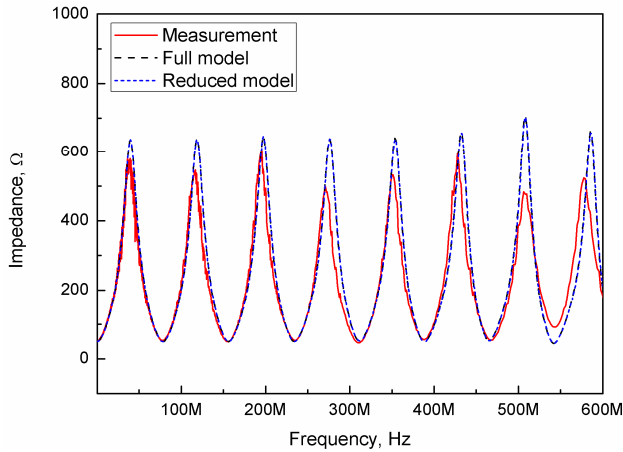


Figure 10. Measurement and numerical results by full mesh and selective mesh.

Table 2. Computation consumption of the full model and reduced model.

	Total number of		Consumed time (sec)	
	Nodes	Partial elements	Element calculation	Circuit solver
Full model	270	55006	161.9	819.2
Reduced model ($k = 0.95$)	148	13349	31.6	32.1

Table 2 shows the numbers of unknowns and the consumed time of the full model and the reduced model. It is evident that the consumed time of the element calculation and circuit solving of the reduced model in this example is only 1/5 and 1/25 of the counterparts of the full model. Numerous practical applications indicate that both the number of unknowns and the consumed time are reduced using the proposed selective mesh approach.

5. CONCLUSION

A selective mesh approach which is consistent with coupled field distribution is proposed for PEEC modeling in this paper. The intense coupling parts are meshed while the remaining parts are eliminated. The resulting meshed region of ground plane is dependent on the length

and height of the above wires in wire-ground structures. Numerical results show that the mesh approach can greatly reduce the unknowns while preserving the sufficient precision, which follows the reduction of consumed modeling time. This approach especially has potentials for wiring analysis in aspect of system EMC and can be extend to other equivalent circuit modeling techniques.

ACKNOWLEDGMENT

This work was supported in part by the National Natural Science Foundation of China (No. 60831001) and Innovation Foundation of BUAA for PhD Graduates. The authors would also like to thank China Scholarship Council (CSC) for offering the first author a precious research opportunity in France.

REFERENCES

1. Paul, C. R., *Introduction to Electromagnetic Compatibility*, 2nd edition, John Wiley & Sons, Hoboken, New Jersey, 2006.
2. Kong, L. and M. Luo, "Co-frequency interference suppression algorithm via maximum signal minus interference level," *Progress In Electromagnetics Research*, Vol. 104, 183–199, 2010.
3. Tsai, H.-C., "Investigation into time- and frequency-domain EMI-induced noise in bistable multivibrator," *Progress In Electromagnetics Research*, Vol. 100, 327–349, 2010.
4. Ding, T.-H., Y.-S. Li, X. Yan, and Y.-Z. Qu, "A new efficient method for calculation and suppression of simultaneous switching noise with the time-domain impedance function for high-speed circuit design," *Progress In Electromagnetics Research*, Vol. 112, 41–62, 2011.
5. Paul, C. R., *Analysis of Multiconductor Transmission Lines*, 2nd edition, Wiley-IEEE Press, New York, 2007.
6. Roy, A., S. Ghosh, and A. Chakraborty, "Simple crosstalk model of three wires to predict near-end and far-end crosstalk in an EMI/EMC environment to facilitate EMI/EMC modeling," *Progress In Electromagnetics Research B*, Vol. 8, 43–58, 2008.
7. Kirawanich, P., J. R. Wilson, N. E. Islam, and S. J. Yakura, "Minimizing crosstalks in unshielded twisted-pair cables by using electromagnetic topology techniques," *Progress In Electromagnetics Research*, Vol. 63, 125–140, 2006.

8. Huang, W.-T., C.-H. Lu, and D.-B. Lin, "Suppression of crosstalk using serpentine guard trace vias," *Progress In Electromagnetics Research*, Vol. 109, 37–61, 2010.
9. FAR25, *Airworthiness Standards: Transport Category Airplanes*, FAA, Washington DC, 2007.
10. Ruehli, A. E., "Equivalent circuit models for three dimensional multiconductor systems," *IEEE Transactions on Microwave Theory and Techniques*, Vol. 22, No. 3, 216–221, Mar. 1974.
11. Ruehli, A. E. and A. C. Cangellaris, "Progress in the methodologies for the electrical modeling of interconnects and electronic packages," *Proceedings of the IEEE*, Vol. 89, No. 5, 740–771, May 2001.
12. Antonini, G., "The partial element equivalent circuit method for EMI, EMC and SI analysis," *ACES Newsletter*, Vol. 21, No. 1, 8–32, Mar. 2006.
13. Song, Z., D. Su, F. Duval, and A. Louis, "Model order reduction for PEEC modeling based on moment matching," *Progress In Electromagnetics Research*, Vol. 114, 285–299, 2011.
14. Vahrenholt, V., H. D. Bruns, and H. Singer, "Reduction of unknowns in PEEC structures by exploiting connectivity of PEEC cells," *IEEE Transactions on Electromagnetic Compatibility*, Vol. 49, No. 2, 412–418, May 2007.
15. Bern, M. and P. Plassmann, *Mesh Generation, Handbook of Computational Geometry*, Elsevier Science, 2000.
16. Fernandez-Recio, R., L. E. Garcia-Castillo, S. Llorente-Romano, and I. Gomez-Revuelto, "Convergence study of a non-standard schwarz domain decomposition method for finite element mesh truncation in electromagnetics," *Progress In Electromagnetics Research*, Vol. 120, 439–457, 2011.
17. Antonini, G., M. D. Prinzio, A. Petricola, and A. E. Ruehli, "Reduced unknowns meshing for the partial element equivalent circuit approach," *International Symposium on Electromagnetic Compatibility*, Chicago, Illinois, Aug. 2005.
18. Ekman, J., G. Antonini, and A. E. Ruehli, "Impact of partial element accuracy on PEEC model stability," *IEEE Transactions on Electromagnetic Compatibility*, Vol. 48, No. 1, 19–32, Feb. 2006.
19. Song, Z., W. Yahyaoui, F. Duval, and D. Su, "Capturing skin effect with an effective non-uniform mesh and coupled R-L circuits," *Electronics Letters*, Vol. 47, No. 2, 94–95, Jan. 2011.
20. Harrington, R. F., *Field Computation by Moment Methods*, 2nd edition, Wiley-IEEE Press, 1993.

21. Shi, Y. and C. H. Liang, "Simulations of the left-handed medium using discontinuous Galerkin method based on the hybrid domains," *Progress In Electromagnetics Research*, Vol. 63, 171–191, 2006.
22. Verbeek, M. E., "Partial element equivalent circuit (PEEC) models for on-chip passives and interconnects," *International Journal of Numerical Modelling*, Vol. 17, No. 1, 61–84, Feb. 2004.
23. Ho, C., A. E. Ruehli, and P. Brennan, "The modified nodal approach to network analysis," *IEEE Transactions on Circuits and Systems*, Vol. 22, No. 6, 504–509, Jun. 1975.
24. Sadiku, M. N. O., *Numerical Techniques in Electromagnetic*, 2nd edition, CRC Press, New York, 2001.
25. Nabors, K. and J. White, "FastCap: A multipole accelerated 3-D capacitance extraction program," *IEEE Transactions on Computer-aided Design of Integral Systems*, Vol. 10, No. 11, 1447–1459, Nov. 1991.
26. Kamon, M., M. J. Tsuk, and J. White, "FASTHENRY: A multipole-accelerated 3-D inductance extraction program," *IEEE Transactions on Microwave Theory and Techniques*, Vol. 42, No. 9, 1750–1758, Sep. 1994.
27. Long, H., "Partial element equivalent circuit method for three-dimensional full-medium systems and its modeling," Ph.D. Thesis, Tsinghua University, 2005.
28. Jackson, J. D., *Classical Electrodynamics*, 3rd edition, John Wiley & Sons, New York, 1998.
29. Lim, J., J. Lee, J. Lee, S. Han, D. Ahn, and Y. Jeong, "A new calculation method for the characteristic impedance of transmission lines with modified ground structures or perturbation," *Progress In Electromagnetics Research*, Vol. 106, 147–162, 2010.
30. Liu, Y., L. Tong, W. Zhu, Y. Tian, and B. Gao, "Impedance measurements of nonuniform transmission lines in time domain using an improved recursive multiple reflection computation method," *Progress In Electromagnetics Research*, Vol. 117, 149–164, 2011.
31. Antonini, G., D. Deschrijver, and T. Dhaene, "Broadband macromodels for retarded partial element equivalent circuit (rPEEC) method," *IEEE Transactions on Electromagnetic Compatibility*, Vol. 49, No. 1, 35–48, Feb. 2007.